Particles from Volcanic Scoria Powders: Granulometry and Granulomorphology Data Analysis

Willy Hermann Juimo Tchamdjou[1]*, Azzeddine Bouyahyaoui[2], Moulay Larbi Abidi[2], Toufik Cherradi[2] and Didier Fokwa[3]

[1]*Department of Civil Engineering and Architecture, National Advanced School of Engineering, University of Maroua, Maroua, Cameroon*

[2]*Department of Civil Engineering, Mohammed School of Engineers, Mohammed V University of Rabat, Rabat, Morocco*

[3]*Department of Civil Engineering, Higher Technical Teachers' Training College, University of Douala, Douala, Cameroon*

Keywords: Volcanic scoria powder, particle, granulometry, granulomorphology and data analysis.

Abstract: This study presents size and shape parameters relevant to volcanic scoria powder characterization. Particle size distribution was compared using two different techniques, including laser diffraction and automated static image analysis, and their respective results were discussed. Specific information on particle shape has been obtained using image analysis by 2-D images. The image analysis was used to identify key controls on particle morphology, six shape parameters: elongation, circularity, solidity, roughness, bluntness and luminance have effectively accounted for the morphological variance of powder particles. The effect of the number of particles of testing samples on these variables obtained through the image analysis was investigated. To develop analytical models, Multiple linear regressions analysis was applied using the dataset. The dataset comprised size and shape information's about 24,268 particles from black natural powder, 32,302 particles from dark red natural powder, 22,562 particles from red natural powder and 25,041 particles from yellow natural powder. The analysis allowed us to identify the explanatory variables and develop eight mathematical models and three of these models are intended to prediction with very good significance. The correlation coefficients and analysis of variance test results obtained evidence the adequacy level of models. Thus, it is possible to estimate each dependent response parameter through the proposed models.

1 INTRODUCTION

In the past few years, several studies have been published that focused on the characterization of maximum packing of supplementary cementitious materials (SCMs) in cement-based systems. The related works generally classified the factors that affect the matrix compactness into four groups: particle morphology, particle packing, interparticle spacing and matrix rheology (Felekoglu. 2009; Arvaniti et al, 2015a; Bouyahyaoui et al, 2018). Particle size and particle shape are closely related to the reactivity of SCMs. Industrial by-products, their partial replacement of cement in concrete mixes represents a substantial offset by the consequent environmental impact. The size and shape characterization of irregular particles is a key issue in many fields of science (Bagheri et al, 2015) and engineering (food, pharmaceutics, minerals, biology, astronomy, …), which is often associated with large uncertainties (Felekoglu. 2009; Bouyahyaoui et al, 2018; Bagheri et al, 2015; Liu et al, 2015; Dioguardi et al, 2018). The main characteristics of powders are the particle size (granulometry) and particle shape (morphology). Technological properties of powders depend on their granulometry and particle morphology (Pavlović et al, 2010).

To date, only a few studies have been published on particle size and particle shape parameters of mineral powders using as SCMs (Felekoglu. 2009; Bouyahyaoui et al, 2018; Bagheri et al, 2015 ; Hackley et al, 2004 ; Michel and Courard, 2014 ; Klemm and Wiggins, 2017). Technological properties of mineral powders (bulk density, flowability, surface area, etc.), as well as the potential areas of SCMs, depend on these characteristics (Mikli et al, 2001). It also has been known that powders may improve the particle packing density of cementitious system, and superplasticizers help to obtain the desired rheological properties by increasing the workability without causing segregation in fresh state (Bouglada et al, 2019) and improve the mechanical properties and durability by reducing the water/cement ratio. Some of these powder materials are either industrial by-products or unprocessed materials. They provide environmental relief because industrial by-products are being recycled and hazardous emissions released into the atmosphere due to cement production are reduced, raw materials are preserved and energy is saved (Felekoglu. 2009). Besides, inert and semi-inert powders such as grounded volcanic scoria can be alternatively employed for high-performance mortar and concrete mixture designs (Juimo et al, 2017). More recent works have addressed the effects of volcanic scoria powder addition on rheological properties of cement paste (Bouglada et al, 2019; Tchamdjou et al, 2017a; Tchamdjou et al, 2017b).

Powders are problematic materials in the application of particle size analysis (Felekoglu. 2009). In general, sizing techniques work best over a limited size range. The optimum range of particle size analysis varies according to many factors, including detector sensitivity and the assumptions associated with the underlying principle of measurement (Felekoglu. 2009; Arvaniti et al, 2015b).

Most commercial methods are designed specifically for a range of particle size, and work best with homogeneous spheres. The degree to which irregularity affects the results vary with the technique employed, and is not well understood or exactly accounted for in many methods (Felekoglu. 2009; Bagheri et al, 2015 ; Orhan et al, 2004; Ferraris et al, 2002).

The morphology of raw powder includes its particle size distribution (PSD), specific surface area (S_{SB} or S_{SL}) and particle shape. The PSD can be determined by sieves analysis, laser diffraction (LD) and image analysis (IA). The industrial method to determine S_{SB} is Blaine Air Permeability test (Arvaniti et al, 2015a; Niesel. 1973). The evaluation of particle shape needs complex techniques such as the LD and the IA (Bagheri et al, 2015; Arvaniti et al, 2015b). Individual particle features should be captured by IA to derive the shape descriptors (Bouyahyaoui et al, 2018; Abazarpoor et al, 2017; Ilic et al, 2015).

In this study, the particle shape and surface morphology of volcanic scoria powders (ground at different grades) data were analyzed.

2 EXPERIMENTAL DATA

2.1 Powders Samples

Four volcanic scoria groups according to the color of scoria have been collected. The collected sample was firstly sieved using the 5 mm stainless steel sieve of 20 cm diameter to separate large volcanic scoria (5–100 mm in order) to fine volcanic scoria (≤5 mm). The volcanic scoria sample was performed on the material dried in an open air environment during 24 h and in the oven at 105 °C during 24 h for the removal of moisture in the rocks (Juimo et al, 2016).

The mill process was performed for 20 minutes. Milling sample has been introduced at the same weight for each production. The rotation speed of the mill was about 70 rpm (Bouyahyaoui et al, 2018). Each powder obtained has been described by a two-component code designation: the letter reflecting powder color as black (B), dark-red (DR), red (R) and yellow (Y) followed by the ‘np’ reflecting natural powder or natural pozzolan (Juimo et al, 2017).

2.2 Measurement Methods

2.2.1 Gas Pycnometer and Blaine Air Permeability (Blaine Fineness, BF)

In this work, the density of powders was performed on a Gas Pycnometer. This method measures the density by determining the volume of inert gas that can be introduced into a sample chamber of a defined size which contains a known mass of powder. Automatic Gas Pycnometer has long been identified as the instrument of choice to accurately measure the true density of solid materials by employing Archimedes’ principle of fluid displacement, and Boyle’s Law of gas expansion (Niesel. 1973; EN 196-6, 2010). Helium inert gas, rather than a liquid, is used since it will penetrate even the finest pores and eliminate the influence of surface chemistry. This ensures quick results of the highest accuracy.

The fineness of the grinding was being determined according to the Blaine technique and is indicated as the specific surface (Blaine fineness value). The Blaine Air Permeability apparatus serves exclusively for the determination of the specific surface area (S_{SB}) of powders. The Blaine Fineness (BF) value is not a measure of granulometric distribution (Means PSD).

2.2.2 Laser Diffraction (LD)

The granulometry of powders was determined by many methods (sieve analysis, LD, IA, etc.), but the question is how adequately they describe the powder granulometry (Mikli et al, 2001). Mikli et al. (Mikli et al, 2001) reported that the evaluation of the fine powder granulometry (with particle size less than 50 µm) is more difficult and the results of the sieve analysis do not describe adequately the powder granulometry. For this reason, the first method used here to describe powder granulometry is LD. LD which is based on a complex theory of interaction between monochromatic light and individual particles. This involves the detection of the angular distribution of light scattered by a set of monodispersed spherical particles to provide a 'sphere'-equivalent size diameter distribution using a reverse optical scattering-based model calculation (Michel and Courard, 2014).

In LD, the angular distribution of light is measured after passing through an optically dilute dispersion of suspended particles. The LD system determines the PSD based on a volumetric basis. Different optical models are commonly used to build the PSD weighted by apparent volume (volume of an equivalent sphere of diameter D), such as Mie theory-based and Fraunhofer models (Michel and Courard, 2014; Varga et al, 2018).

2.2.3 Image Analysis (IA)

IA has made a decisive breakthrough in the recent years to become a reference technique in the field of combined size and shape analysis of particles (Arvaniti et al, 2015b; Gregoire et al, 2007). The IA is a method for the measurement of particle size and shape distributions. For the measurement of particle size and morphometric characterization, an Occhio 500 Nano image analyzer has been used. The morphology of a powder particle is characterized by shape description (elongation, circularity, solidity, roughness, bluntness (with the calypter), luminance) or quasi-quantitatively, for example, by means of geometrical shape parameters.

The IA is based on the measurement of each particle; the accuracy of a size and shape distribution has to be formulated in number of particles (N_P) and not in terms of sample weight or duration of the analysis. The adequate particle number is linked to the shape of the distribution curve and its extension or range (Gregoire et al, 2007). Volcanic scoria powders tested by the IA had respectively: 24,268 particles for Bnp, 32,302 particles for DRnp, 22,562 particles for Rnp and 25,041 particles for Ynp.

3 DATA ANALYSIS METHODS

Data sets obtained by experimental analysis were studied using SPSS software to understand the influence and the correlation of different considerable parameters (factors). The analysis of the individual influence of a given factor in the description of a complex phenomenon, such as the max distance (X_{DM}) or geodesic length (X_{LG}) of the powder particle can lead to erroneous conclusions; for example a given factor could seem extremely relevant when it is not. Slinker and Glantz (Slinker and Glantz, 2008) and Neves et al. (Neves et al, 2018) reported that, a given variable may appear unrelated to the dependent variable when analyzed alone, but may have a strong influence when considered simultaneously with other predictors. To model and identify the main factors that influence the other size parameter descriptors in particle max distance and geodesic length, a multiple linear regression (MLR) analysis is used, which makes if possible examine the simultaneous effects of multiple of independent predictor variables (IPVs) in the variability of the dependent or explained variable (Neves et al, 2018).

Table 1: Definitions of response variables and IPVs in the systems.

Variable/Definition			
Y or Y_i	Max Distance (X_{DM}), Geodesic length (X_{LG}), Powdering ratio index by Blaine ($Pr_{SB} = N_P/(S_{SB} \times D_S)$) or Powdering ratio index by LD ($Pr_{SL} = N_P/(S_{SL} \times D_S)$).		
Var.	*Definition*	*Variable*	*Definition*
x_1	Inner Diameter (X_{DI})	y_1	Elongation (E_l)
x_2	Area Diameter (X_{DA})	y_2	Circularity (C_c)
x_3	Width (W_b)	y_3	Solidity (S_d)
x_4	Length (L_b)	y_4	Roughness (R_g)
x_5	Max Distance (X_{DM})	y_5	Luminance (L_m)
x_6	Geodesic length (X_{LG})	y_6	Bluntness (B_t)

This study also aimed to evaluate the potential relationship between dependent variables (i.e., X_{DM} ; X_{LG} ; Pr_{SB} or Pr_{SL}) and input variables (i.e., X_{DI}; X_{DA}; W_b; L_b; X_{DM}; X_{LG}; E_l; C_c; S_d; R_g; L_m; B_t) by applying statistical models. The independent variables Pr_{SB} and Pr_{SL} expresses by $N_P/(S_{SB} \times D_S)$ and $N_P/(S_{SL} \times D_S)$, and represent powdering ratio index of powders by BF and LD respectively.

The explanatory variables included in models are : X_{DI}; X_{DA}; W_b; L_b; X_{DM}; X_{LG}; E_l; C_c; S_d; R_g; L_m and B_t. Besides the conventional linear regression model, introduced as Model 1(with 4 IPVs) and Model 2 (with 5 IPVs) in Equation (1) based on the linear regression model provide by Neves et al. (Neves et al, 2018) and Jin et al. (Jin et al, 2018).

$$Y = f(x_i) \rightarrow Y \; = \alpha_0 + \sum_{i=1}^{n} \alpha_i x_i + \varepsilon = \alpha_0 + \alpha_1 x_1 + \alpha_2 x_2 + \cdots + \alpha_n x_n + \epsilon \quad (1)$$

where Y represents the dependent variable (also called response variable, output, endogenous or explained), α_0 , α_1 , . . ., α_k the regression coefficients, $x_1, x_2,$ . . ., x_k the IPVs (Table I) and ϵ the random errors of the model.

Table 2: Description of the multiple linear regression model.

Equation /Model n°		IPVs used to predict Max Distance (X_{DM})	IPVs used to predict Geodesic length (X_{LG})	IPVs used to predict Powdering ratio index by Blaine ($Pr_{SB} = N_P/(S_{SB} \times D_S)$)	IPVs used to predict Powdering ratio index by LD ($Pr_{SL} = N_P/(S_{SL} \times D_S)$)
Eq. (1)	1	X_{DI}, X_{DA}, W_b, L_b	-	-	-
	2	$X_{DI}, X_{DA}, W_b, L_b, X_{LG}$	$X_{DI}, X_{DA}, W_b, L_b, X_{DM}$	-	-
Eq. (2)	3	X_{DI} , $X_{DI} \times E_l$, $X_{DI} \times C_c$, $X_{DI} \times R_g$, $X_{DI} \times S_d$, $X_{DI} \times L_m$, $X_{DI} \times B_t$			
	4	X_{DA} , $X_{DA} \times E_l$, $X_{DA} \times C_c$, $X_{DA} \times R_g$, $X_{DA} \times S_d$, $X_{DA} \times L_m$, $X_{DA} \times B_t$			
	5	W_b , $W_b \times E_l$, $W_b \times C_c$, $W_b \times R_g$, $W_b \times S_d$, $W_b \times L_m$, $W_b \times B_t$			
	6	L_b , $L_b \times E_l$, $L_b \times C_c$, $L_b \times R_g$, $L_b \times S_d$, $L_b \times L_m$, $L_b \times B_t$			
	7	-	X_{DM} , $X_{DM} \times E_l$, $X_{DM} \times C_c$, $X_{DM} \times R_g$, $X_{DM} \times S_d$, $X_{DM} \times L_m$, $X_{DM} \times B_t$		
	8	X_{LG} , $X_{LG} \times E_l$, $X_{LG} \times C_c$, $X_{LG} \times R_g$, $X_{LG} \times S_d$, $X_{LG} \times L_m$, $X_{LG} \times B_t$	-	X_{LG} , $X_{LG} \times E_l$, $X_{LG} \times C_c$, $X_{LG} \times R_g$, $X_{LG} \times S_d$, $X_{LG} \times L_m$, $X_{LG} \times B_t$	

The regression equation given by Equation (1) gives the value predicted for the dependent variable according to the IPVs included in the model, which lies on the best-fit regression plane, which represents the multidimensional generalization of a line (Slinker and Glantz, 2008; Neves et al, 2018).

In this research we also proposed alternative non-linear models to improve the determination coefficients when predicting dependent variables (Model 1 & 2: Multi-linear regression analysis).

These models range from Model 3 to Model 8 in Equation (2), where $i = 1, \cdots, 6$ denotes the number of IPVs concerning particle size descriptors. The analysis of the interactions between size and shape parameters in the description the max distance or geodesic length of the powder particle, a MLR analysis is used, which allows examining the simultaneous effects of multiple IPVs in the variability of the dependent or explained variable with variables interact.

The statistical relationship between the dependent variable Y_i and the multiple IPVs x_i and y_k is given by Equation (2) (Model 3 to 8: Non-linear model involving variables interactions).

$$Y_i = f(x_i, y_j) \rightarrow Y_i \; = \beta_0 + \sum_{j=1}^{k} \beta_j x_i y_j + \varepsilon \; = \; \beta_0 + \beta_1 x_i y_1 + \beta_2 x_i y_2 + \cdots + \beta_k x_i y_k + \epsilon \quad (2)$$

where Y_i represents the dependent variable (also called response variable, output, endogenous or explained, $i = 1, \cdots, n$), β_0 , β_1 , . . ., β_k the regression coefficients, x_i and y_1 , x_2 ,. . ., y_k the independent variables (Table 1) and ε the random errors of the model.

The regression equation given by Equation (2) gives the value predicted for the dependent variable according to the IPVs included in the model which lies on the best-fit regression plane that represents the multidimensional generalization of a line (Slinker and Glantz, 2008; Neves et al, 2018).

Among the k independent predictor variables (IPVs), some may have more significant effects on the target response variable than others as reported by Jin et al. (Jin et al, 2018). In the same way, the t-test of correlation analysis was used to determine the significance regarding the effect of each IPV on the response variable in this study. There is a p-value corresponding to each t-value for an IPV. At the 95% confidence level, a p-value lower than 0.05 would indicate that this selected IPV makes a significant contribution to the response variable. In contrast, IPVs with p-values higher than 0.05 are those without significant contributions. A possible reason why some IPVs had higher significance than others was the strong internal correlation among IPVs, which caused redundancies. Therefore, the regression analysis could be redone by removing the redundant IPVs, shortening the equation to include only significant IPVs. Target models, response variables and various IPVs using input systems are defined in Table 1 and Table 2.

Figure 1: Summary of production process and main testing data of powders.

4 RESULTS AND DISCUSSION

4.1 Principal Properties

The powders obtained have a density between 2.8 and 3.1 g/cm^3 and SSA Blaine between 3,500 and 5,300 cm^2/g, which are comparable to ordinary Portland cement fineness ((Bouyahyaoui et al, 2018; Juimo et al, 2017).

By LD, mean particle diameter (Dmed), mean particle diameter of 10% of particles D(10), median particle diameter D(50) and mean particle diameter of 90% of particles D(90) were measured to evaluate the efficiency of the milling process. Using the PSD data obtain by LD and Equations (1)-(2), S_{SL} evaluated are ranging between 4,400 to 6,000 cm^2/g. S_{SL} value obtains by this method for each powder is always higher, that is about 4% to 25% than S_{SB} obtain by BF (Figure 1).

PSDs of powders were evaluated by using the LD and IA (Figure 1). In the LD technique, the angular distribution of light is measured after passing through an optically dilute dispersion of suspended particles. This technique is widely used in dust and mineral industry with water and dispersive agent to a special cell where the laser light is sent (Felekoglu, 2009; Orhan et al, 2004).

The inscribed disk diameter (X_{DI} or X_{DA}) of each particle is calculated in real time to build PSD curves weighted by apparent volume (Gregoire et al, 2007), making the assumption that particles have identical flatness ratios, whatever their size (Michel and Courard, 2014). Area diameter of particles was used to plot PSD curve obtained by IA. The PSD profile shows a negligible difference in the results by the two methods (Abazarpoor et al, 2017). The main reasons for differences between two PSD methods are as follows: the considerate particle diameter by each measurement process, the different shapes of the particles; better insight into particles using the IA method; insufficient dispersion of fine particles; fine particles adhering to the bigger particles. LD and 2D projection image by the IA are commonly used the PSD measurement techniques, but the results may not be representative of the strongly true physical dimensions of the particles (Califice et al, 2013).

4.2 Particle Morphology Analysis

More than 50 images of powder particles were identified. The particle morphology was found to provide reasonable accuracy for estimating the particle sizes of highly porous particles, where the distinction between inter-particle and intra-particle porosity was made. This important comment concerning inter-particle and intra-particle porosity has been also reported by Klemm and Wiggins (Klemm and Wiggins, 2017).

4.2.1 Particle Morphology: Size Parameters Distribution

Figure 2 shows the general identification of particles according to their inner diameter and area diameter. About 25% of Bnp particles, 25% of Ynp particles, 25% of DRnp particles, 25% of Bnp and 5% of Bnp particles have the same area diameter like respectively a particle n°1, n°2, n°3, n°4 and n°5 as showing in Figure 2. In the same way, about 5% of DRnp particles, 5% of Bnp particles, 6% of Rnp particles, 6% of Ynp and 25% of Ynp particles have the same area diameter like respectively a particle n°1, n°2, n°3, n°4 and n°5 as showing in Figure 2.

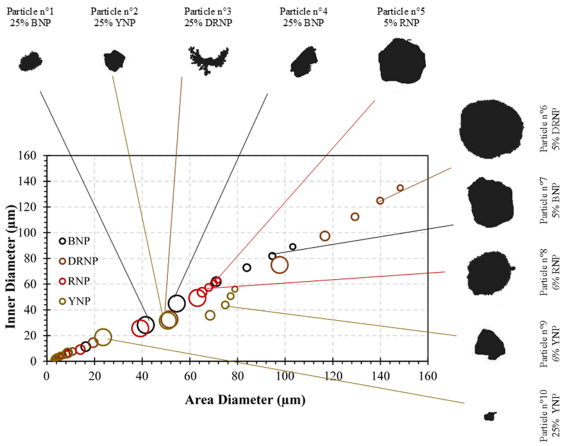

Figure 2: Identification of particles based on their inner diameter and area diameter.

Particles who have a high inner diameter and area diameter are from DRnp powder and Particles who present a very few inner diameter and area diameter are from Rnp and Ynp powders.

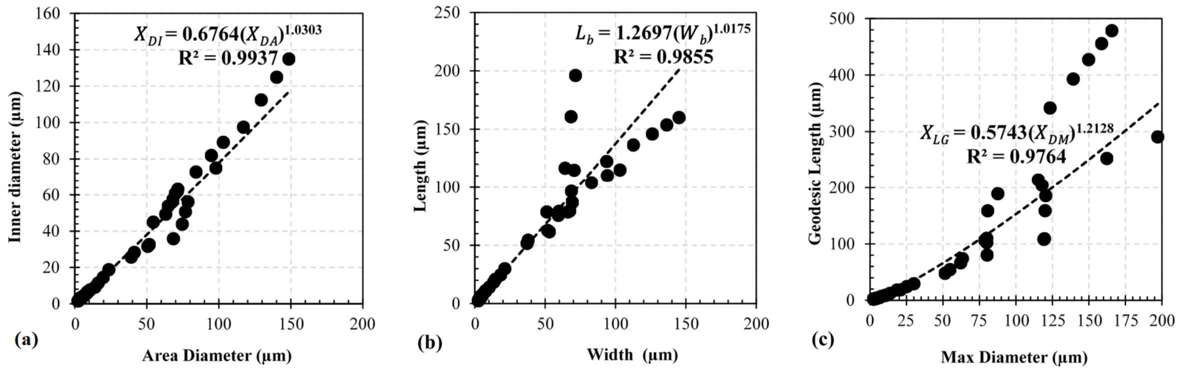

Figure 3: Relation between (a) inner and area diameter, (b) width and length and (c) max distance and geodesic length consider all powders.

Figure 3a shows that for all data obtained for all powders, inner diameter and area diameter are well related with a coefficient of correlation up to 0.99.

Figure 4 shows the general identification of particles according to their inner diameter and area diameter. About 25% of Bnp particles, 25% of DRnp particles, 25% of Bnp particles, 6% of Ynp and 5% of Bnp particles have the same width as particles n°11, n°12, n°13, n°9 and n°7 respectively as shown in Figure 4.

In the same way, about 5% of DRnp particles, 5% of Rnp particles, 25% of Rnp particles, 25% of Rnp and 25% of Ynp particles have the same length as particles n°6, n°14, n°8, n°15 and n°16 respectively as also shown in Figure 4. Particles that have a higher width are from DRnp powder and those that present a higher length are from Ynp powder. Particles that present a very few width and length are from Rnp and Ynp powders. Figure 3b shows that for all data obtained for all powders, width and length are well related with a coefficient of correlation up to 0.98.

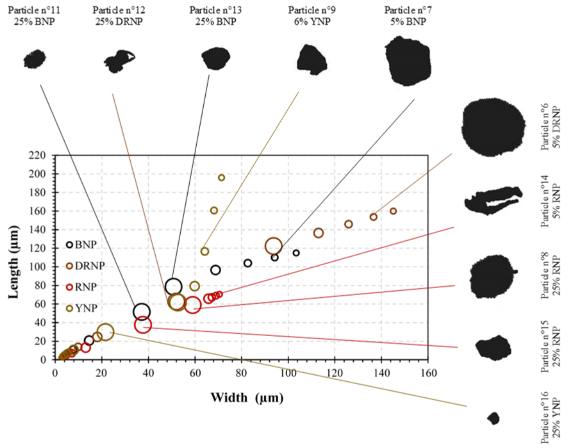

Figure 4: Identification of particles based on their width and length.

Figure 5 shows the general identification of particles according to their max distance and geodesic length. About 25% of Bnp particles, 25% of DRnp particles, 25% of Bnp particles, 5% of Rnp and 5% of DRnp particles have the same max distance as particles n°11, n°17, n°18, n°14 and n°6 respectively as shown in Figure 5. In the same way, about 5% of Ynp particles, 5% of Bnp particles, 25% of Rnp particles, 25% of Rnp and 25% of Ynp particles have the same geodesic length as particles n°19, n°20, n°21, n°22 and n°23 respectively as also shown in Figure 5.

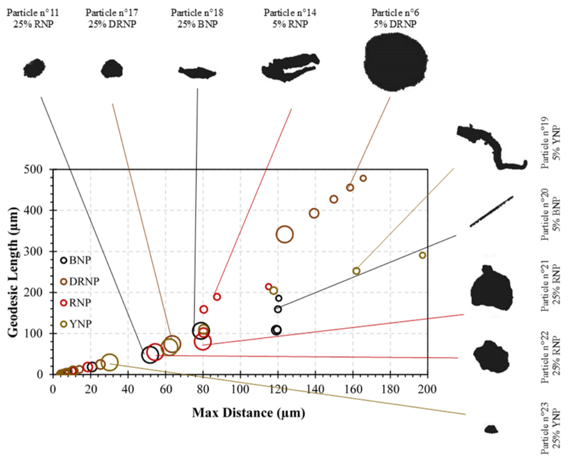

Figure 5: Identification of particles based on their max distance and geodesic length.

Particles that have a higher max distance are from DRnp and Ynp powders and whose who present a higher geodesic length are from DRnp powder. Particles that present a very few max distance and geodesic length are from Rnp and Ynp powders.

Figure 3c shows that for all data obtained for all powders, max distance and geodesic length are well related with a coefficient of correlation up to 0.97.

4.2.2 Particle Morphology: Shape Parameters Distribution

Figure 6 shows the general identification of particles according to their elongation and circularity. About 4% of DRnp particles, 9% of Bnp particles, 25% of Ynp particles, 25% of DRnp and 6% of Ynp particles have the same circularity as particles n°6, n°24, n°25, n°26 and n°27 respectively as shown in Figure 6.

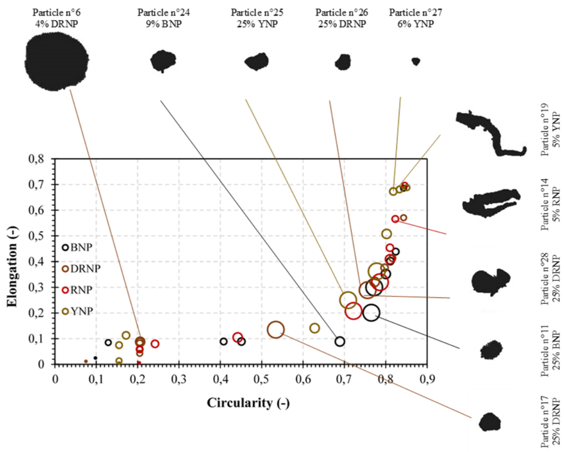

Figure 6: Identification of particles based on their elongation and circularity.

In the same way, about 5% of Ynp particles, 5% of Rnp particles, 25% of DRnp particles, 25% of Bnp and 25% of DRnp particles have the same elongation as particles n°19, n°14, n°28, n°11 and n°17 respectively as also shown in Figure 6. Particles that have a higher elongation are from Rnp and Ynp powders and those that present a higher circularity are from Rnp and Ynp powders. Particles that present a very few elongation and circularity are from Bnp and DRnp powders.

Figure 7 shows the general identification of particles according to their roughness and solidity. About 6% of Bnp particles, 6% of DRnp particles, 5% of DRnp particles, 5% of Rnp and 6% of Ynp particles have the same roughness as particles n°29, n°30, n°31, n°32 and n°19 respectively as shown in Figure 7.

In the same way, about 25% of Rnp particles, 25% of DRnp particles, 25% of Ynp particles, 25% of Bnp and 25% of DRnp particles have the same solidity as particles n°33, n°17, n°25, n°7 and n°6 respectively as also shown in Figure 7. Particles that have a higher roughness are from Ynp powder. Particles that present a very few roughnesses are also from Ynp powder. These powder particles have in general a solidity value equal to 1.0. This means that these particles from volcanic scoria have a higher solidity.

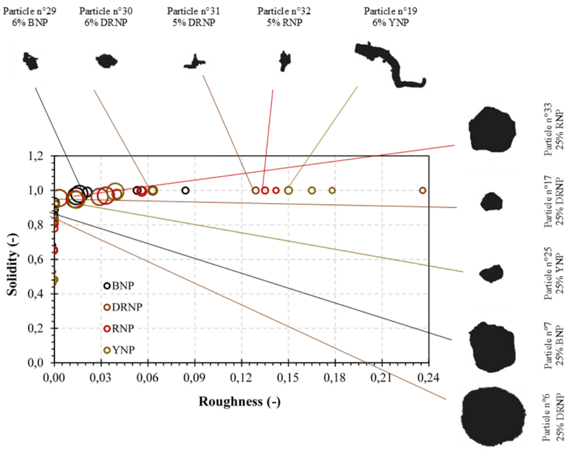

Figure 7: Identification of particles based on their roughness and solidity.

Figure 8 shows the general identification of particles according to their luminance and bluntness. About 4% of DRnp particles, 5% of Bnp particles, 25% of Rnp particles, 25% of Ynp and 5% of Rnp particles have the same bluntness as particles n°34, n°35, n°36, n°16 and n°37 respectively as shown in Figure 8.

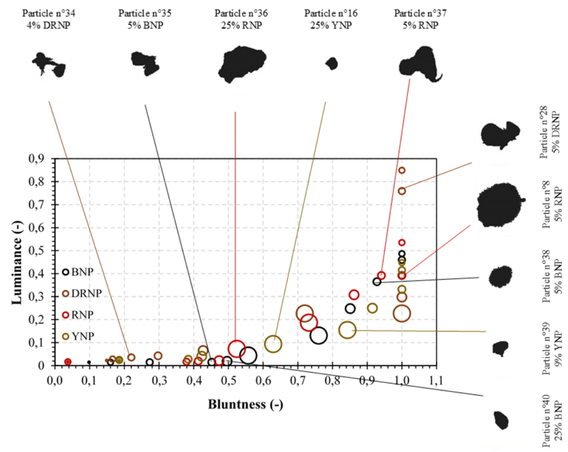

Figure 8: Identification of particles based on their luminance and bluntness.

In the same way, about 5% of DRnp particles, 5% of Rnp particles, 5% of Bnp particles, 9% of Ynp and 25% of Bnp particles have the same luminance as particles n°28, n°8, n°38, n°39 and n°40 respectively as also shown in Figure 8. Particles that have a higher luminance are from DRnp powder. Particles that present a very few luminance are from Rnp and Bnp powders.

4.3 Study the Correlation Between Several Parameters

In this study, the two major input systems within volcanic scoria powder particle morphology (i.e., size and shape input systems) were compared for their accuracy in predicting considered dependent variable. In addition, the effect of number of particle projections (N_P) on the variables obtained through IA is investigated.

The bestfit models were identified under each input system. By removing significantly correlated IPVs within each input system, the regression modelling process was rerun by shortlisting (Jin et al, 2018).

Figure 9 presents the summary of measurement values for size and shape parameters of powder sample identifying the variables considered in this study. These data are used for the definition of several models, to predict the considerable dependent variable. These values have obtained the consideration of 24,268, 32,302, 22,562 and 25,041 particles for Bnp, DRnp, Rnp and Ynp respectively. For all size parameters, the value is down to 500 µm for all powders.

The regression analysis was conducted based on the proposed models for input systems, respectively. The reliability of these models was compared, and the best-fit model was identified. Table 3 displays the corresponding R^2 values for all predictions. The summary of models is shown in Table 3 where the statistical coefficients analyzed are presented to evaluate the validity of the regression model. The model proposed for samples leads a correlation coefficient (R) of 0.810 and a determination coefficient (R^2) of 0.779, thus revealing a very strong correlation between the values predicted by the model and the values observed in the dataset.

Table 3 shows also the analysis of variance (ANOVA) of models. The ANOVA table reveals an F value (Fisher-Snedecor test) of models, which is considerably higher than the critical value of F, for a level of significance of 5%. Moreover, the significance value of the model is practically null, thus lower than the p-value adopted as significance level (5%). The results obtained reveal that all the independent variables considered are statistically significant in explaining the dependent variable.

As shown in Table 3, input systems led to highly consistent R^2 values (up to 0.919) from Models 1 to 8 for predicting X_{DM} and X_{LG} , meaning similar prediction accuracy. Model 4 (the mixed model using size/shape as the RRV) achieved the consistently high R^2 values for all the four predicted variables (X_{DM}, X_{LG}, Pr_{SB} or Pr_{SL}).

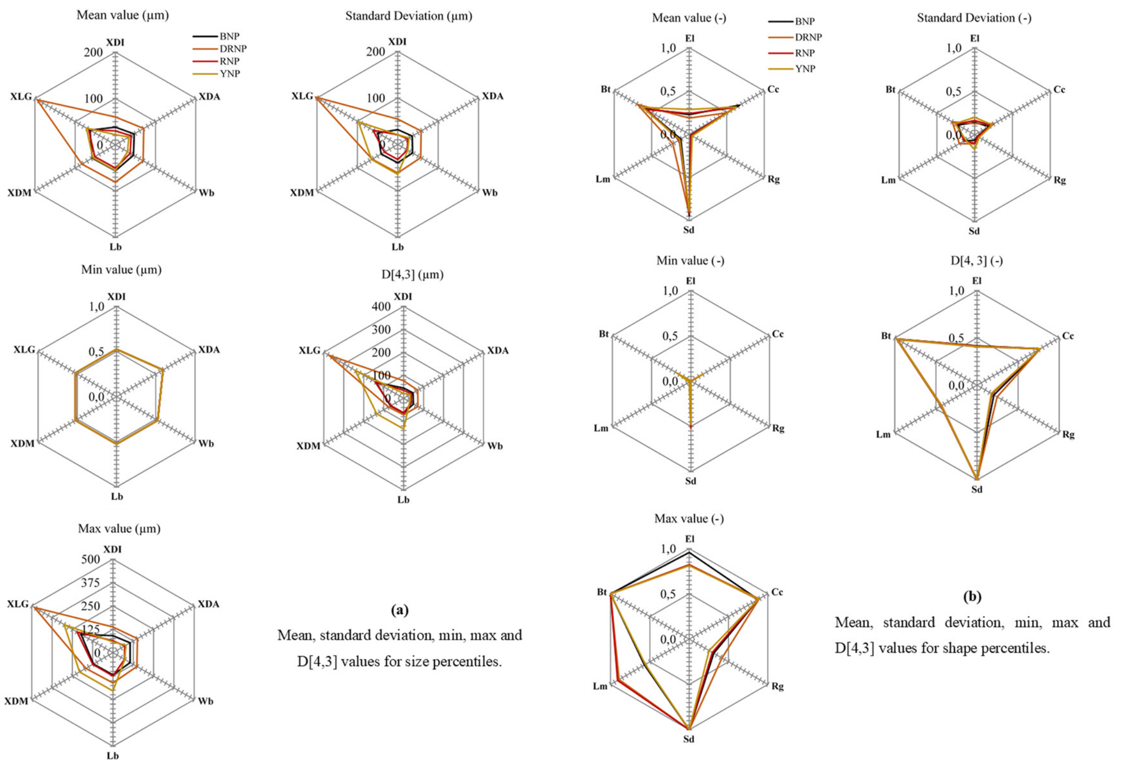

Figure 9: Summary of measurement values for size and shape parameters of powders.

All of the corresponding R^2 values in the 25 scenarios are within the reasonable range (i.e., 0.810–0.998). Model 1 also achieved the highest R^2 value for the prediction of X_{DM} in both systems (0.998 for Multi-linear regression analysis and 0.979 for Non-linear model involving variables interactions).

In the Pr_{SB} or Pr_{SL} regression analysis, Model 6 (the non-linear approach) represents the best-fit model by achieving even higher accuracy than others, the highest based on both input systems.

The remaining mixed models had relatively lower R^2 values for both input systems. The R^2 values resulting from the best-fit non-linear and mixed regression models in this research (ranging from 0.810–0.998) are significantly higher than the values generated from previous studies adopting linear methods. This can be seen in Table 3.

According to these correlation and ANOVA coefficients, model 2, model 5 and model 6 are the three best models to predict max distance and geodesic length and the best model to predict Powdering ratio index by Blaine and by LD is the model 6 as indicated in bold in Table 3.

The linear regression coefficients (α_i or β_j) of the proposed models were determinate. All the independent variables included in the model are statistically relevant in the description of the variability of the dependent variable, showing a significance value lower than the p-value (5%). The linear regression coefficients of model present a significance value lower than the p-value (5%), indicating that all the independent variables are statistically relevant in the description of the dependent response n coefficient obtained from this test technique (Table 4). These significance values are marked in green and the models selected on this basis are also marked in bold in Table 4. According to these p-values, model 2 and model 5 are the two best models to predict max distance and geodesic length and the best model to predict Powdering ratio index by Blaine and by LD is the model 6 as indicated in bold in Table 4.

Once the statistical relevance of models is confirmed, Table 5 presents the mathematical formulation that makes rating estimation of each dependent response possible.

Table 3: Summary of the multiple linear regression analysis results (In this table, *Analysis of variance of the model (ANOVA), **Square of the mean square error (RMSE))

Parameter			Correlation				ANOVA*	
Eq.	Model n°		R	R^2	R^2ad.	RMSE**	F value	p value
Equation (1)	1	X_{DM}	0.998	0.996	0.996	3.868045369	2436.723	0.000
	2	X_{DM}	**0.999**	**0.998**	**0.997**	**2.963935818**	**3325.711**	**0.000**
		X_{LG}	**0.972**	**0.944**	**0.944**	**34.390131493**	**128.921**	**0.000**
Equation (2)	3	X_{DM}	0.942	0.888	0.866	21.326295389	40.846	0.000
		X_{LG}	0.959	0.919	0.904	42.540114280	58.587	0.000
		Pr_{SB}	0.951	0.904	0.885	0.286212210	48.326	0.000
		Pr_{SL}	0.945	0.892	0.871	0.244277238	42.594	0.000
	4	X_{DM}	0.968	0.936	0.924	16.097413373	75.576	0.000
		X_{LG}	0.969	0.939	0.927	36.948598108	79.335	0.000
		Pr_{SB}	0.944	0.891	0.870	0.304327341	42.150	0.000
		Pr_{SL}	0.946	0.896	0.876	0.240259398	44.204	0.000
	5	X_{DM}	**0.989**	**0.979**	**0.974**	**9.349541278**	**234.136**	**0.000**
		X_{LG}	**0.980**	**0.960**	**0.952**	**29.887883900**	**123.964**	**0.000**
		Pr_{SB}	**0.942**	**0.888**	**0.866**	**0.308774263**	**40.798**	**0.000**
		Pr_{SL}	**0.944**	**0.892**	**0.871**	**0.244995796**	**42.314**	**0.000**
	6	X_{DM}	**0.998**	**0.996**	**0.996**	**3.787558166**	**1452.888**	**0.000**
		X_{LG}	**0.979**	**0.959**	**0.951**	**30.442169551**	**119.306**	**0.000**
		Pr_{SB}	**0.931**	**0.866**	**0.840**	**0.337897319**	**33.220**	**0.000**
		Pr_{SL}	**0.936**	**0.876**	**0.852**	**0.261645598**	**36.467**	**0.000**
	7	X_{LG}	0.973	0.947	0.937	34.388965646	92.379	0.000
		Pr_{SB}	0.930	0.864	0.838	0.340304620	32.679	0.000
		Pr_{SL}	0.935	0.873	0.849	0.264888669	35.454	0.000
	8	X_{DM}	0.966	0.934	0.923	16.211425615	86.685	0.000
		Pr_{SB}	0.900	0.810	0.779	0.396643132	26.314	0.000
		Pr_{SL}	0.903	0.815	0.785	0.315815860	27.153	0.000

According to these equations with higher correlation (Table 5), including main characteristics of powders: the particle size, particle shape and technological properties of powders (density, surface area, etc.). It is demonstrated that using powders, as well as the potential areas of their application, strongly depends on these characteristics. Dimensionless relationships between particle size and particle shape can be determined theoretically for simplified, but realistic, powder particle geometries. These relationships have important implications for the interpretation of shape data, and, more fundamentally, for the selection of grain size(s) for analysis.

5 CONCLUSIONS

This study showed that the size estimation of particulate material is a complicated matter. The results highlight the fact that particle size distributions may not be unique. Different techniques can give a large range of different parameters which need to be interpreted correctly. The choice of the parameters also depends on the purpose of the research. It is shown that particle shape analysis that includes the full range of available grain sizes can contribute not only measurements of particle size and shape, but also information on size-dependent densities and specific surface area.

Based on the analysis of particle characteristics, design of experiment, and analysis of variance (ANOVA), it can be concluded that: good correlation was found between the specific surface area measured by Blaine Permeability Tester and calculated from the LD and the IA data.

Thus, based on these conclusions, it appears that the density, specific surface area, granulometry and, morphology of volcanic scoria powders may be efficiently estimated from complementary techniques. This description is absolutely needed for understanding particles' behavior in contact with water when used in cementitious materials.

ACKNOWLEDGEMENTS

The first author would like to thank Mrs. Sophie Leroy and Mr. Frédéric Michel, GeMMe research engineers at the University of Liège (Belgium) for their help in the testing program.

REFERENCES

Abazarpoor, A., Halali, M., Hejazi, R., Saghaeian, M., 2017. *HPGR effect on the particle size and shape of iron ore pellet feed using response surface methodology*, Mineral Processing and Extractive Metallurgy, pp. 1-9.

Arvaniti, E. C., Juenger, M. C. G., Bernal, S. A., Duchesne, J., Courard, L., Leroy, S., Provis, J. L., Klemm, A., De Belie, N., 2015a. *Physical characterization methods for supplementary cementitious materials*, Materials and Structures, 48(11):3675–3686.

Arvaniti, E. C., Juenger, M. C. G., Bernal, S. A., Duchesne, J., Courard, L., Leroy, S., Provis, J. L., Klemm, A., De Belie, N., 2015b. *Determination of particle size, surface area, and shape of supplementary cementitious materials by different techniques*, Materials and Structures, 48(11):3687–3701.

Bagheri, G. H., Bonadonna, C., Manzella, I., Vonlanthen, P., 2015. *On the characterization of size and shape of irregular particles*, Powder Technology, 270:141–153.

Bouglada, M. S., Naceri, A., Baheddi, M., Pereira-de-Oliveira, L., 2019. *Characterization and modelling of the rheological behaviour of blended cements based on mineral additions*, European Journal of Environmental and Civil Engineering, pp. 1-18.

Bouyahyaoui, A., Cherradi, T., Abidi, M. L., Tchamdjou, W. H. J., 2018. *Characterization of particle shape and surface properties of powders from volcanic scoria*, Journal of Materials and Environmental Science, 9(7):2032-2041.

Califice, A., Michel, F., Dislaire, G., Pirard, E., 2013. *Influence of particle shape on size distribution measurements by 3D and 2D image analyses and laser diffraction*, Powder Technology, 237:67–75.

Dioguardi, F., Mele, D., Dellino, P., 2018. *A new one-equation model of fluid drag for irregularly shaped particles valid over a wide range of Reynolds number*, J. of Geophysical Res.:Solid Earth, 123:144–156.

EN 196-6., 2010. *Methods of testing cement - Part 6: Determination of fineness*, European Standard.

Felekoglu, B., 2009. *A new approach to the characterisation of particle shape and surface properties of powders employed in concrete industry*, Construction and Building Materials, 23:1154–1162.

Ferraris, C. F., Hackley, V. A., Aviles, A. I., Buchanan, C. E., 2002. *Analysis of the ASTM round-Robin test on particle size distribution of Portland cement: Phase I*, Report no. 6883. Maryland: National Institute of Standards and Technology (NISTIR).

Gregoire, M. P., Dislaire, G., Pirard, E., 2007. *Accuracy of size distributions obtained from single particle static digital image analysis*, Proceeding. PARTEC Conference. Nürenberg, 4p.

Hackley, V. A., Lum, L-S., Gintautas V., Ferraris, C. F., 2004. *Particle size analysis by laser diffraction spectrometry: application to cementitious powders*, Report no. 7097. Maryland: National Institute of Standards and Technology (NISTIR).

Ilic, M., Budak, I., Vucinic, M., Nagode, A., Kozmidis-Luburic, U., Hodolic, J., Puskar, T., 2015. *Size and shape particle analysis by applying image analysis and laser diffraction-inhalable dust in a dental laboratory*, Measurement, 66:109–117.

Jin, R., Chen, Q., Soboyejo, A. B. O., 2018. *Non-linear and mixed regression models in predicting sustainable concrete strength*, Construction and Building Materials, 170:142–152.

Juimo, W. H. T., Grigoletto, S., Michel, F., Courard, L., Cherradi, T., Abidi., M. L., 2017. *Effects of various amounts of natural pozzolans from volcanic scoria on performance of Portland cement mortars*, International Journal of Engineering Research in Africa, 32:36-52.

Juimo, W., Cherradi, T., Abidi, L., Oliveira, L., 2016. *Characterisation of natural pozzolan of "Djoungo" (Cameroon) as lightweight aggregate for lightweight concrete*, GEOMATE, 11(27):2782-2789.

Klemm, A. J., Wiggins, D. E., 2017. *Particle size characterisation of SCMs by mercury intrusion porosimetry*, Fizyka Budowli W Teorii I Praktyce Tom IX, Nr 1-2017, pp 5-12.

Liu, E. J., Cashman, K. V., Rust., A. C., 2015. *Optimising shape analysis to quantify volcanic ash morphology*, GeoResJ, 8:14–30.

Michel, F., Courard, L., 2014. *Particle size distribution of limestone fillers: granulometry and specific surface area investigations*, Particulate Science and Technology, 32:334-340.

Mikli, V., Käerdi, H., Kulu, P., Besterci, M., 2001. *Characterization of powder particle morphology*, Proceedings of the Estonian Academy of Sciences, Engineering 7(1):22–34.

Neves, R., Silva, A., De Brito, J., Silva, R.V., 2018. *Statistical modelling of the resistance to chloride penetration in concrete with recycled aggregates*, Construction and Building Materials, 182 : 550–560.

Niesel, K., 1973. *Determination of the specific surface by measurement of permeability*, Materials and Structures, 6(3):227-231.

Orhan, M., Özer, M., Işık, N., 2004. *Investigation of laser diffraction and sedimentation methods which are used for determination of grain size distribution of fine grained soils*, G.U. Journal of Science, 17(2):105–113.

Pavlović, M. G., Pavlović, L. J., Maksimović, V. M., Nikolić, N. D., Popov, K. I., 2010. *Characterization and morphology of copper powder particles as a function of different electrolytic regimes*, International Journal of Electrochemical Science, 5:1862–187.

Slinker, B. K., Glantz, S.A., 2008. *Multiple linear regression: accounting for multiple simultaneous determinants of a continuous dependent variable*, Circulation, 117(13):1732–1737.

Tchamdjou, W. H. J., Abidi, M. L., Cherradi, T., De Oliveira, L. A. P., 2017a. *Effect of the color of natural pozzolan from volcanic scoria on the rheological properties of Portland cement pastes*, Energy Procedia, 139:703–709. DOI: 10.1016/j.egypro.2017.11.275.

Tchamdjou, W. H. J., Cherradi, T., Abidi, M. L., De Oliveira, L. A. P., 2017b. *Influence of different amounts of natural pozzolan from volcanic scoria on the rheological properties of Portland cement pastes*, Energy Procedia, 139:696–702. DOI: 10.1016/j.egypro.2017.11.274.

Varga, G., Kovács, J., Szalai, Z., Cserháti, C., Újvári, G., 2018. *Granulometric characterization of paleosols in loess series by automated static image analysis*, Sedimentary Geology, 370, pp 1-14.

Table 4: p-value (In this table, x : non-considered variable, xx : excluded variable).

Model n°		Const.	X_{DI}	X_{DA}	W_b	L_b	X_{DM}	X_{LG}	$X_{DI} \times E_l$	$X_{DI} \times C_c$	$X_{DI} \times R_g$	$W_b \times S_d$	$W_b \times L_m$	$W_b \times B_t$
X_{DM}	1	0.842	0.226	0.610	0.864	0.000	x	x	x	x	x	x	x	x
X_{DM}	**2**	**0.121**	**0.001**	**0.304**	**0.107**	**0.000**	**x**	**0.000**	**x**	**x**	**x**	**x**	**x**	**x**
X_{LG}		**0.008**	**0.000**	**0.030**	**0.006**	**0.000**	**0.000**	**x**	**x**	**x**	**x**	**x**	**x**	**x**
X_{DM}	3	0.365	x	0.120	x	x	x	x	0.001	0.946	0.038	0.199	0.442	0.203
X_{LG}		0.289	x	0.046	x	x	x	x	0.969	0.796	0.903	0.034	0.355	0.000
Pr_{SB}		0.279	x	0.405	x	x	x	x	0.584	0.261	0.543	0.234	0.155	0.009
Pr_{SL}		0.160	x	0.287	x	x	x	x	0.863	0.198	0.772	0.159	0.109	0.002
Model 4		Const.	X_{DI}	X_{DA}	W_b	L_b	X_{DM}	X_{LG}	$X_{DA} \times E_l$	$X_{DA} \times C_c$	$X_{DA} \times R_g$	$X_{DA} \times S_d$	$X_{DA} \times L_m$	$X_{DA} \times B_t$
X_{DM}		0.365	x	0.120	x	x	x	x	0.001	0.946	0.038	0.199	0.442	0.203
X_{LG}		0.289	x	0.046	x	x	x	x	0.969	0.796	0.903	0.034	0.355	0.000
Pr_{SB}		0.279	x	0.405	x	x	x	x	0.584	0.261	0.543	0.234	0.155	0.009
Pr_{SL}		0.160	x	0.287	x	x	x	x	0.863	0.198	0.772	0.159	0.109	0.002
Model 5		**Const.**	X_{DI}	X_{DA}	W_b	L_b	X_{DM}	X_{LG}	$W_b \times E_l$	$W_b \times C_c$	$W_b \times R_g$	$W_b \times S_d$	$W_b \times L_m$	$W_b \times B_t$
X_{DM}		**0.110**	**x**	**x**	**0.094**	**x**	**x**	**x**	**0.000**	**0.265**	**0.000**	**0.042**	**0.000**	**0.667**
X_{LG}		**0.748**	**x**	**x**	**0.169**	**x**	**x**	**x**	**0.000**	**0.757**	**0.000**	**0.105**	**0.907**	**0.000**
Pr_{SB}		0.334	x	x	0. 605	x	x	x	0.885	0.267	0.944	0.358	0.023	0.002
Pr_{SL}		0.118	x	x	0.249	x	x	x	0.870	0.182	0.462	0.130	0.001	0.001
Model 6		Const.	X_{DI}	X_{DA}	W_b	L_b	X_{DM}	X_{LG}	$L_b \times E_l$	$L_b \times C_c$	$L_b \times R_g$	$L_b \times S_d$	$L_b \times L_m$	$L_b \times B_t$
X_{DM}		0.519	x	x	x	0.966	x	x	0.908	0.386	0.330	0.313	0.400	0.384
X_{LG}		0.783	x	x	x	0.261	x	x	0.001	0.952	0.084	0.185	0.336	0.000
Pr_{SB}		**0.035**	**x**	**x**	**x**	**0.070**	**x**	**x**	**0.041**	**0.246**	**0.523**	**0.042**	**0.510**	**0.049**
Pr_{SL}		**0.012**	**x**	**x**	**x**	**0.028**	**x**	**x**	**0.091**	**0.183**	**0.533**	**0.017**	**0.260**	**0.017**
Model 7		**Const.**	X_{DI}	X_{DA}	W_b	L_b	X_{DM}	X_{LG}	$X_{DM} \times E_l$	$X_{DM} \times C_c$	$X_{DM} \times R_g$	$X_{DM} \times S_d$	$X_{DM} \times L_m$	$X_{DM} \times B_t$
X_{LG}		0.906	x	x	x	x	0.281	x	0.002	0.931	0.061	0.208	0.603	0.000
Pr_{SB}		0.037	x	x	x	x	0.092	x	0.035	0.325	0.349	0.056	0.371	0.078
Pr_{SL}		0.013	x	x	x	x	0.040	x	0.078	0.255	0.352	0.023	0.176	0.030
Model 8		**Const.**	X_{DI}	X_{DA}	W_b	L_b	X_{DM}	X_{LG}	$X_{LG} \times E_l$	$X_{LG} \times C_c$	$X_{LG} \times R_g$	$X_{LG} \times S_d$	$X_{LG} \times L_m$	$X_{LG} \times B_t$
X_{DM}		0.399	x	x	x	x	x	0.076	0.010	0.111	0.136	xx	0.390	0.000
Pr_{SB}		0.182	x	x	x	x	x	0.127	0.939	0.021	0.570	xx	0.499	0.000
Pr_{SL}		0.122	x	x	x	x	x	0.160	0.585	0.011	0.460	xx	0.351	0.000

Table 5: Equations of efficient models identified.

Model n°	Equations	R^2
Model 2	$X_{DM} = -1.167 + 0.435X_{DI} + 0.281X_{DA} - 0.501W_b + 1.043L_b - 0.056X_{LG}$	0.998
	$X_{LG} = -22.528 + 6.003X_{DI} + 6.718X_{DA} - 9.542W_b + 8.240L_b - 7.590X_{DM}$	0.944
Model 5	$X_{DM} = 6.306 - 4.455W_b - 1.989W_b \times E_l + 0.827W_b \times C_c + 4.877W_b \times R_g + 5.815W_b \times S_d - 1.377W_b \times L_m + 0.157W_b \times B_t$	0.979
	$X_{LG} = -3.989 + 11.619W_b - 6.019W_b \times E_l + 0.727W_b \times C_c + 8.110W_b \times R_g - 14.650W_b \times S_d - 0.053W_b \times L_m + 7.069W_b \times B_t$	0.960
Model 6	$Pr_{SB} = 0.302 - 0.145L_b - 0.031L_b \times E_l + 0.024L_b \times C_c + 0.025L_b \times R_g + 0.175L_b \times S_d - 0.006L_b \times L_m - 0.021L_b \times B_t$	0.866
	$Pr_{SL} = 0.282 - 0.137L_b - 0.019L_b \times E_l + 0.021L_b \times C_c + 0.019L_b \times R_g + 0.162L_b \times S_d - 0.008L_b \times L_m - 0.020L_b \times B_t$	0.876